ISSN 1063-7710, Acoustical Physics, 2009, Vol. 55, No. 6, pp. 741–753. © Pleiades Publishing, Ltd., 2009.

OCEAN ACOUSTICS. HYDROACOUSTICS

Specific Features of Estimation of Levels and Spatial Spectrum of Ocean Noise by a Single Multicomponent Combined Receiver

V. A. Gordienko[a], N. V. Krasnopistsev[b], A. V. Nasedkin[b], V. N. Nekrasov[b], and V. N. Toropov[b]

[a] *Faculty of Physics, Moscow State University, Moscow, 119992 Russia*
e-mail: vgord@list.ru

[b] *FSUE Research Institute of Physicotechnical and Radio Engineering Measurements, Mendeleevo, Moscow oblast, 141570 Russia*

Received November 28, 2006; in final form, February 9, 2009

Abstract—Algorithms for estimation of the spatial spectrum of ocean noise using a single hydroacoustic combined receiving module (CRM), which records the field of acoustic pressure and its gradient projections onto three mutually orthogonal spatial directions for small wave sizes, are discussed. It is shown that in spite of a rather "obtuse" cosine directional response pattern of vector channels of this receiving module it is possible to obtain good determination of the direction toward the local source due to recording the vector characteristic of the acoustic field (acoustic power flux), and in the absence of powerful local sources in the water area the spatial spectrum of noise close to a realistic one can be obtained.

PACS numbers: 43.30.Wi, 43.58.Fm

DOI: 10.1134/S1063771009060086

1. INTRODUCTION

Increasing interest in small-size hydroacoustic systems including an acoustic pressure receiver (omnidirectional hydrophone) and the vector receiver has been observed recently both in our country and abroad [1–4]. This is related with the fact that known methods and algorithms based on the application of information recorded by pressure receivers have reached their limiting capabilities, as it regards recording signals of local sources with the signal-to-noise ratio (SNR) at the input much smaller than unity [2, 5, 6]. Such small-size receiving systems are usually called combined receiving modules (CRMs) or combined receivers if the omnidirectional hydrophone and the vector receiver are combined in one frame.

In scientific journals, including the Russian Acoustic Journal (see, e.g., [7–10], papers, in which the capabilities of different CRM designs are analyzed, appear regularly. However, real algorithms for the combined processing of signals recorded from separate channels of such receiving systems in the general case are not discussed. Usually, characteristics of solitary channels are used for analysis which is not always correct. This circumstance is explained by the fact that for obtaining the spatial distribution of the vibrational speed's vector it is necessary to record simultaneously two (planar case) or three (volume problem) projections of this vector without amplitude–phase distortions, and for the Umov vector, additionally acoustic pressure. Thus, actually, the fact that the single multicomponent CRM can record other measurements than the pressure field's physical characteristics of the acoustic field called vector characteristics is ignored. As a result, there appears the possibility of realizing quite novel approaches to the analysis of recorded signals which, on the one hand, make the capabilities of this receiving system close to those of the antenna array based on hydrophones, and on the other hand, make CRM fundamentally different from the latter [1, 11, and 12].

It should be noted that a single CRM cannot completely replace an extended antenna array based on hydrophones in the investigation of spatial noise spectra of a water area (see [12, 13]). Spatial distribution of the acoustic power flux's vector can be used for estimation (and only estimation) of the spatial noise spectrum of a water area with certain constraints for solution of particular applied problems. This is especially topical for the low frequency and subsonic ranges for which it is difficult to create antenna arrays with "good" spatial resolution.

In this paper an attempt is made to analyze basic specific features of signal processing algorithms which use the recorded vector of the acoustic power flux. Without substantiating the concept of vector–phase methods (see [1] for detail) we consider the capabilities of these methods in solution of one of the fundamental problems, the estimation of the level and spatial spectrum of the noise of a water area.

2. TWO APPROACHES TO PROCESSING SIGNALS RECORDED BY CRMS

Two fundamentally different approaches to processing signals received from separate CRM channels can be separated. The first approach includes the so called *additive algorithms* which provide the formation within one receiving module of the dipole or close to the cardioid's directional response patterns oriented in a given direction. Further signal processing (including from the point of view of noise immunity) does not fundamentally differ from processing signals received from common hydrophones for which basic estimates of noise immunity described in literature (e.g., [8–10]) based on the idea of the concentration factor of a receiving system [13, 14] are applicable. Algorithms of estimation of the noise anisotropy in the water area using additive algorithms were considered in [1, 11].

The second approach is related with *nonlinear signal processing* which looks similar to the multiplicative or correlation processing. Here, recording of the acoustic energy flux and its reactive component are separated.

The total acoustic power (energy) of flux vector is usually determined as the product of in-phase components of instantaneous acoustic pressure and vibrational speed (Umov vector) [14], averaged over some time τ multiple or much larger than the oscillation period of the medium particles in the wave, i.e.,

$$\mathbf{W}_\mathrm{R} = \overline{P(t)\mathbf{V}(t)}\big|_\tau \equiv \frac{1}{\tau}\int_0^\tau P(t)\mathbf{V}(t)dt.$$

Hereinafter, the symbol "$\overline{\ldots}$" denotes averaging over time, and "$\langle\ldots\rangle$" averaging over the ensemble. The projection $W_{\mathrm{R}r}$ of the vector $\mathbf{W}_\mathrm{R}$ onto the direction $\mathbf{r}$ characterized by the projection of the vibrational speed $V_r(t)$ is determined by the following expression: $W_{\mathrm{R}r} = \frac{1}{\tau}\int_0^t P(t)V_r(t)dt$. In particular, for the narrow-band (quasiharmonic) signal $W_{\mathrm{R}r} = \frac{1}{2}P_0V_{0r}\cos(\Delta\varphi_{PV}) = \frac{1}{2}\mathrm{Re}(P^*V_r) = \frac{1}{4}(PV_r^* + P^*V_r)$, where $\Delta\varphi_{PV}$ is the phase difference between the pressure and the projection of the vibrational speed with the amplitudes P_0 and V_{0r}, respectively, the symbol "*" denotes the complex conjugate's quantity.

The projection $W_{\mathrm{I}r}$ of the vector of reactive component of the acoustic power flux's density (density of reactive acoustic energy) onto the direction $\mathbf{r}$ is determined as the time-averaged product of instantaneous acoustic pressure and the phase-shifted by $\pi/2$ with respect to it component of the vibrational speed's projection. For the quasiharmonic signal,

$$W_{\mathrm{I}r} = \frac{1}{2}P_0V_{0r}\sin\Delta\varphi_{PVr}$$

$$= \frac{1}{2}\mathrm{Im}(P^*V_r) = \frac{1}{4}(P^*V_r - PV_r^*).$$

At present, the reactive component of the acoustic energy flux is measured quite seldom, although in principle some possible aspects of its use are described in the literature [1, 2, and 15].

Nonlinear-type algorithms also include the combined processing when first the cardioid with the output signal U_k is formed (it provides an offset from the local noise's source), and then, the spectra of the combinations (V_x, U_k) and (V_y, U_k) are determined. This algorithm is not discussed here.

3. ALGORITHMS FOR ESTIMATION OF SPATIAL SPECTRUM OF ACOUSTIC FIELDS BASED ON THE MEASUREMENT OF THE ACOUSTIC POWER FLUX'S PROJECTIONS

It is assumed quite reasonably that the spatial spectrum of the signal (spatial intensity distribution) can be determined with the help of the spatial array of sound receivers (antenna). The number of sound receivers N and their spatial position in the antenna determine the number of elements of the orthonormal expansion basis and actually the angular resolution of the antenna according to Raleigh's criterion. Modern processing methods provide increased spatial resolution of angularly localized sources (super-resolution effect), however, they require additional constraints to be imposed on the signal, which in the general case, do not always agree with real conditions (see, e.g., [16, 17]). Therefore, the error probability for obtaining the spatial spectrum in the case of super-resolution is as a rule higher.

A single CRM formally does not allow calculation of the spatial spectrum of the wave vector $\mathbf{k}(\omega, r)$ [18], but it provides the possibility of its estimation using measurements in the spatial domain considerably smaller than the wavelength. In the framework of this paper we describe the simplest possible algorithm for analysis of the spatial distribution of the absolute value of the vector of the acoustic power flux $\mathbf{W}_\mathrm{R}$ implemented by us in practice; this method, however, requires rather high computer power. It is important that for this algorithm the spatial resolution is not directly connected with the concentration factor of the directional response patterns of the vector receiver but is determined by physical (mainly statistical) specific features of formation of the vector of the acoustic power flux, the noise vector, and the localized sources in the water area [1, 19].

It was shown earlier (see, e.g., [1, 11]) that for the localized source in the layer the following relations are satisfied: $P^2 \approx (\rho c V_r)^2 \approx \rho c W_{\mathrm{R}r}$. This means that the transition to the measurement of the acoustic power flux of angularly localized sources provides a metrologically correct estimation of their levels. If we consider the relatively steady-state (during the time of measurements) noise field of the water area, the vectors $\mathbf{W}_{\mathrm{R}} = \mathbf{i}W_{\mathrm{R}x} + \mathbf{j}W_{\mathrm{R}y} + \mathbf{k}W_{\mathrm{R}z}$ determined at different time instants have different spatial orientation, and their statistical angular distribution is determined by the character of the noise source's anisotropy. Isotropic noise in some frequency regions with the average frequency f the values of $\langle W_{\mathrm{R}i}(f)\rangle$ $(i = x, y, z)$ averaged over different realizations of the ensemble of samples tend to zero with increasing averaging time τ. In the case of anisotropic noise the ratio of the integral averaged over some time interval's values $\gamma_{ai} = \langle W_{\mathrm{R}i}(f)\rangle / \overline{P^2(f)}$ provide the estimation of the relative contribution of the anisotropic noise's field component in the water area for the spatial directions x, y, z, and any other direction $\mathbf{r}$.

If it is possible to obtain a sufficiently large number of independent pairs (for some fixed spatial plane) or trios (volume case) of samples of the projections $W_{\mathrm{R}i}(f)$, the statistical angular distribution of the intensity $I = \sqrt{\sum_i W_{\mathrm{R}i}^2}$ of the acoustic field's energy in the water area can be constructed (here, similar to above, $i = x, y, z$). This statistical processing allows one to judge the *spatial spectrum of the noise field*, in particular, to determine the minimal "necessarily" achievable for the given water area's noise immunity of the applied CRM (with account of more precise determination of this notion, as applied to the receiver recording the acoustic energy flux [1, 12, and 13]) upon transition to recording the acoustic power flux.

The following procedure can be proposed for estimation of the spatial spectrum of the noise of a water area; this procedure is to some extent optimized, although rather cumbersome, and can be implemented in two somewhat different ways.

In the first case (let us call it algorithm I) in the given frequency range Δf including m narrow-band signals with different frequency or frequency subranges δf_i with the average subrange frequency f_i for each sampling with the number q, the array of m independent trios of projections of acoustic power fluxes is constructed, $W_{\mathrm{R}xi} = W_{\mathrm{R}x}(t_q, f_i)$, $W_{\mathrm{R}yi} = W_{\mathrm{R}y}(t_q, f_i)$, $W_{\mathrm{R}zi} = W_{\mathrm{R}z}(t_q, f_i)$. It is assumed that the directions of the axes X, Y, and Z are known. Usually, it requires determination of several parameters. For example, if fast Fourier transform algorithms are used, the following quantities should be determined: the length τ_0 of the separate sampling should be determined; as a rule, this length together with the discretization frequency used upon signal digitization determines the frequency resolution of the spectrum; the time shift $\Delta\tau$ between neighboring processed samplings ($t_{q+1} = t_q + \Delta\tau$, where $\Delta\tau$ usually corresponds to one half or one quarter of the sampling length τ_0); the number N averaged for each frequency values W_{R}, and the averaging law.

Within the unit sampling with the length τ_0 and the number q for each frequency subrange δf_i from the analyzed range Δf, the following quantities can be determined: the azimuthal φ_i and the polar ϑ_i signals' arrival angles in the horizontal and vertical planes, respectively, the intensity I_i of this signal, which represents the absolute value of the vector of the acoustic power flux in the direction determined by φ_i and ϑ_i,

$$\tan\varphi_i = \frac{W_{\mathrm{R}yi}}{W_{\mathrm{R}xi}}, \quad \tan\vartheta_i = \frac{W_{\mathrm{R}zi}}{\sqrt{W_{\mathrm{R}xi}^2 + W_{\mathrm{R}yi}^2}},$$
$$I_i(\varphi_i) = \sqrt{W_{\mathrm{R}xi}^2 + W_{\mathrm{R}yi}^2} \quad (1)$$
$$\text{or} \quad I_i(\varphi_i, \vartheta_i) = \sqrt{W_{\mathrm{R}xi}^2 + W_{\mathrm{R}yi}^2 + W_{\mathrm{R}zi}^2}.$$

The whole range of analyzed angles is divided into M sectors (for example for the planar case of the horizontal plane $M = 360/\Delta\varphi_0$, where $\Delta\varphi_0$ is the chosen spatial resolution). Then, for the given frequency band $\Delta f = \sum_{i=1}^{m} \delta f_i$ consisting of the set of m discrete frequency intervals (band δf_i for each interval) (for example, the frequency resolution of the fast Fourier transform or the transmission band of the narrow-band filter) the discrete set of values (array) $I(\varphi_n)$ for the sampling q is calculated according to the algorithm

$$I_q(\varphi_n) = \sum_{i=1}^{m} I_{qi}[f_i, (n-1)\Delta\varphi_0 \le \varphi_i < n\Delta\varphi_0], \quad (2)$$

where n takes values from 1 to M. If necessary (and if it does not contradict the formulated problem), the result can be reduced to a 1 Hz band by dividing the obtained values of $I_q(\varphi_n)$ by $\sum_{i=1}^{m} \delta f_i$.

Then, the next sampling $(q + 1)$ is considered and the procedure is repeated, thus obtaining the array of values $I_{q+1}(\varphi_n)$ for the next time instant larger than the previous one by $\Delta\tau$, and the results of sequential samples are averaged.

If for some τ_0 the signal recording segment with the length $t_{sm} > \tau_0$ multiple to $\Delta\tau$ is chosen for obtaining the values of projections of acoustic power flux, for example, onto the axes X, Y, for each frequency on the recording length t_{sm} we can obtain $N_{sm} = t_{sm}/\Delta\tau$ samples of the angle φ and the intensity $I(\varphi)$, i.e., the whole of $N_{sm}m$ values of $I(\varphi)$. For decreasing fluctuations based on the obtained data, the histogram of $I(\varphi_n)$ distribution averaged over N_{sm} samples in each of

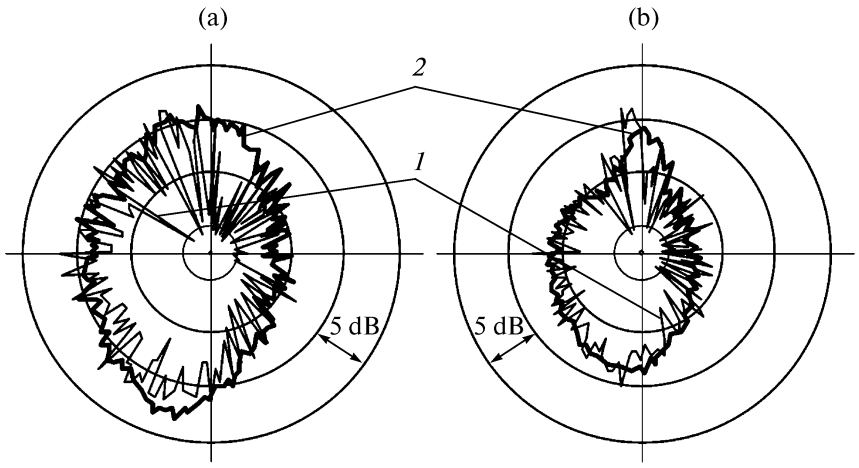

Fig. 1. Anisotropy of background noise of the Gulf of Finland (logarithmic scale) obtained using algorithm I in three-octave frequency ranges (a) 315, (b) 500 Hz for a time resolution of (*1*) 10 and (*2*) 80 s.

M angular sectors is constructed in the analyzed frequency band Δf. This can be common averaging, for example, matched with the length of the analyzed recording fragment t_{sm}. However, if the possible number N of samples (samplings) is not known a priori, or in the case of an online operation (when the sonogram or the 3D diagram is constructed at the output of the data processing system) the exponential averaging law, which yields fast convergence even for the number of samples $q < N = N_{sm}$ [2, 20], should be considered optimal,

$$I(\varphi_n) = \frac{(N_{sm} - 2)I_{q-1}(\varphi_n) + 2I_q(\varphi_n)}{N_{sm}}. \qquad (3)$$

Here, $I(\varphi_n)$ is the value of the current's averaged intensity, $I_q(\varphi_n)$ is the result of determination of the intensity value for the sampling with the number q using formula (2), and $I_{q-1}(\varphi_n)$ is the result of averaging using formula (3) at the previous step. The value N_{sm} is usually chosen to satisfy the steady-state condition for the time interval t_{sm}.

In order to increase the number of unit independent samples, usually the narrow-band spectral analysis is used (for example, choosing the sampling length τ_0 for fast Fourier transforms as large as possible), and the intensity is reduced to the given frequency and angular range by summing the intensities in neighboring frequency bands of the signal. However, in the case for signals with low SNR, problems may occur at the input which will be discussed in the next section.

If $N_{sm}m \gg M$, distribution (3) at the step $q \geq N_{sm}$ can be considered as the *quasispatial spectrum of the acoustic signal for the acoustic power spectrum* in the horizontal plane for the time interval t_{sm}; in the case of absence of powerful localized sources in the water area in the first (rough) approximation it can be close to the spatial spectrum obtained using the horizontal linear antenna. If in this case the vibrational speed is expressed in equivalent units of acoustic pressure of the plane's acoustic wave (i.e., instead of V, the quantity ρcV is considered, where ρc is the wave resistance of the medium), the dimensionalities of I and P^2 coincide, and their numerical values can be compared. In this case for the water area of the type of a layer with impedance boundary, according to data presented in [1], the following condition should be satisfied;

$$\sum_{n=1}^{M} I(\varphi_n) \equiv I_{\Sigma I} \approx P^2. \qquad (4)$$

If the signal was recorded during the time interval considerably larger than t_{sm}, averaging algorithm (3) can be used beginning from $q \approx N_{sm}/2$ and higher to construct the sonogram or the 3D plot of the signal intensity $I(\varphi_n)$ as a function of time with some discrete step Δt determined by the operator at the beginning of processing. Figure 1 shows the example of such distribution $I(\varphi_n)$ of background noise of the Gulf of Finland (the Baltic sea) for third-octave bands of 315 and 500 Hz and N_{sm} corresponding to averaging times of 10 and 80 s ($\delta f_i = 2$ Hz) in the logarithmic scale (dB). Figure 2 shows the example of the sonogram in a frequency band of 140–315 Hz for the case of a dry cargo ship with +6...+8 dB traverse SNR in the pressure channel moving linearly by the CRM installed at a distance of 15 m from the bottom in the shallow water area; the averaging time was 10 s, $\delta f_i = 0.5$ Hz, the depth was about 65 m, and the distance to CRM was about 5 km.

At first glance, it seems that the application of the receiver of the acoustic power flux formally provides spatial resolution. However, it should be taken into account that, unlike antenna arrays, the determination of the spatial intensity's distribution based on the combined processing of the signals $P(\mathbf{r}, t)$ and $\mathbf{V}(\mathbf{r}, t)$

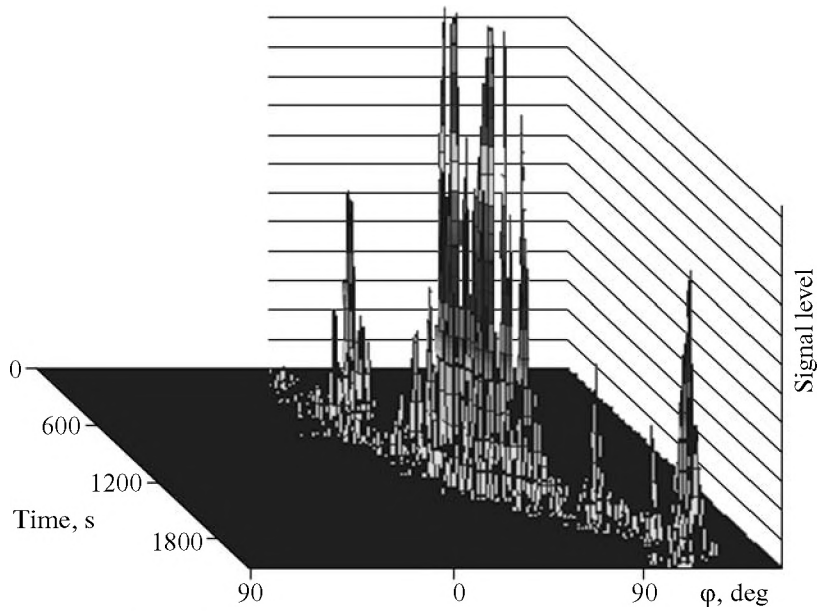

Fig. 2. Example of sonogram in a frequency band of 140–315 Hz (averaging time 10 s, $\delta f_i = 0.5$ Hz) in the presence of a localized source moving with constant velocity in the water area.

assumes signal expansion in the spatial domain in the non-orthogonal basis [1]. Therefore, the obtained spatial distribution of energy input, as a rule, does not necessarily coincide with the true one. The transition to the measurement of projections of the vector of the acoustic power flux partially solves the problem of estimation of the spatial spectrum of the noise of the water area. Actually each operation on the determination of the direction toward the signal (noise) source and its intensity based on the analysis of projections of the vector $\mathbf{W}(\mathbf{r}, t)$ results within one sampling in one value for each analyzed frequency. Therefore, if the initial signal does not fluctuate, it is practically impossible to obtain the spatial intensity's distribution for a separate frequency band. If there exist fluctuations (this situation, as a rule, takes place for the field of self dynamic noise of the ocean) the histogram constructed according to algorithm I begins to reflect the spatial noise's spectrum at the place where the system is situated. However, for reliable statistical estimation a sufficient number of *independent* samples per unit interval of angular resolution $\Delta\varphi$ is required. Thus, for example, for the angular resolution $\Delta\varphi = 1°$ ($M = 360$) statistically reliable results can be obtained if there exist much more than ten independent samples per unit $\Delta\varphi$, i.e., there are at least 4000 samples in the sum. For improving statistics the angular resolution $\Delta\varphi = 2°–3°$ can be taken.

It should be noted that the histogram represents the result of statistical signal processing and reflects the real anisotropy of the water area's noise only in the absence of powerful angularly localized sources. It is in this case that the obtained results can be interpreted as the *spatial spectrum of the water area's noise*.

In the presence of the powerful localized source in the water area the spatial spectrum is distorted. The direction of the "instantaneous" vector $\mathbf{W}_\Sigma$ whose absolute value is determined by the above introduced $I(\varphi)$ at each time instant is determined as the sum of the relatively spatially stable vector $\mathbf{W}_S$ generated by the localized source and the vector $\mathbf{W}_N$ of the field of self noise of the water area distributed according to some random law (Fig. 3), $I(\varphi) = |\mathbf{W}_\Sigma| = |\mathbf{W}_S + \mathbf{W}_N|$.

Indeed, let us consider the behavior of the vector of the acoustic power flux formed by the localized source in the presence of the isotropic noise in the horizontal plane. The signal intensity of such noise per the angular sector $\Delta\varphi$ in the absence of the localized source, processed according to the above algorithm, is determined by the value of the constant P^2/M (Fig. 3c, dependence *1*). If there is the localized source only, it creates at the observation point of the acoustic power flux, which is on average nonzero, and is concentrated in the angular interval determined by expression (1) (Fig. 3c, dependence *2*). Therefore, observing the acoustic field at the only point, one can judge on the direction toward the source (which is the essence of the direction finding problem), rather than the spatial noise's spectrum. In the general case (in the presence of noise and the localized source), the probability's density distribution of the acoustic power flux for the localized source on the background of isotropic noise is described by the Macdonald function [18]. True direction finding for the localized source in this case can be performed by additional processing of the pro-

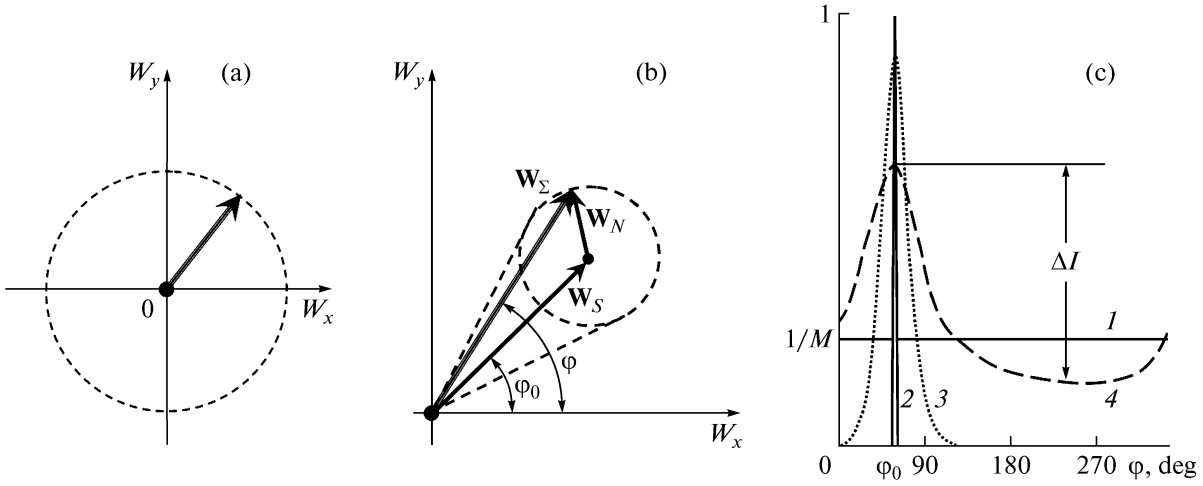

Fig. 3. Formation of spatial statistical distribution of acoustic power flux vector $\mathbf{W}_R$: (a) isotropic noise in horizontal plane; (b) possible angular positions φ in the horizontal plane of the total acoustic power flux vector $\mathbf{W}_\Sigma$ in the presence of a local source forming the acoustic power flux $\mathbf{W}_S$ in the direction φ_0 and isotropic noise $\mathbf{W}_N$ ($W_N < W_S$) in the water area; (c) approximate dependences of the distribution $I(\varphi)$ normalized to P^2 for several typical cases: (*1*) isotropic noise without a local source; (*2*) local source in the absence of noise; (*3*) signal level W_S is much higher than the noise level W_N; (*4*) $W_S \le W_N$.

file of the envelope $I(\varphi)$. The approximate form of the distribution $I(\varphi)$ for finite SNR is shown in Fig. 3c (dependences *3*, *4*). With decreasing SNR the bearing angle's variance increases, and finally the signal excess over the background noise can become comparable with the fluctuation component of the histogram. If there are other localized sources, which also form noise in the water area, the profile of the dependence $I(\varphi)$ is more complex.

The second approach (algorithm II) in its main part coincides with that described above. The difference is in the method of construction of the histogram. Namely, within a separate sampling each corner cell with the number n characterized by the average number of the direction angle φ_n is filled by the intensity, for example, determined by the condition

$$I(\varphi_n) = (1/2)\{[I(\varphi_n) - I(180^\circ + \varphi_n)] + |I(\varphi_n) - I(180^\circ + \varphi_n)|\}.$$

In this case, the *isotropic component of the water area's noise decreases rather fast already for small averaging times* and just relatively space- and time-stable (steady-state) anisotropic components of noise sources remain. This algorithm can be efficiently applied for detection of the source of weak signals on the background of the noise of the water area under the condition that the frequency and angular characteristics of the detected source and "steady-state" components of the noise field do not coincide. The best effect should be obtained in the case of the noise of the water area close to isotropic. In this case the, noise immunity of the receiver recording the vector of the acoustic power flux can considerably exceeds 20 dB [21].

Obviously, the levels of $I(\varphi)$ obtained using algorithms I and II coincide only for localized signal sources whose direction does not change during the processing time. For the field of distributed noise sources usually different levels are obtained. Algorithm II determines the level of the anisotropic component of the acoustic power flux with account of fluctuations (depending on the averaging time); therefore, with increasing the averaging time, τ decreases to this level according to the classical rules. It can be easily shown that for algorithm II, unlike (4), the value $I_{\Sigma II} = \sum_{n=1}^{M} I(\varphi_n) < P^2$. Concerning algorithm I, it contains information on the amplitude and spatial (with account of fluctuations) intensity's distribution and depends on the statistical characteristics of the studied noise field. Therefore, for this algorithm, as it was already indicated above, due to the specific features of formation of the spatial distribution of the vector $\mathbf{W}_R$, the angular dependence $I(\varphi_n)$ does not necessarily coincide with that determined using the extended antenna array. In the case of not more than one or two localized sources in the water area it can be recovered using relatively simple processing algorithms.

The example of processing of this full-scale experiment in the horizontal plane for the White Sea's area (depth of about 300 m) using algorithms I and II in the absence of visible localized sources in the water area are shown in Fig. 4. The angular distribution $I(\varphi)$ normalized to the integral value P^2 for $M = 360$ (angular resolution of 1°) constructed using algorithm I corresponds to the statistical spatial distribution of the vector $\mathbf{W}_R$ of the water area's noise at the point of installation of the receiving system in the horizontal plane.

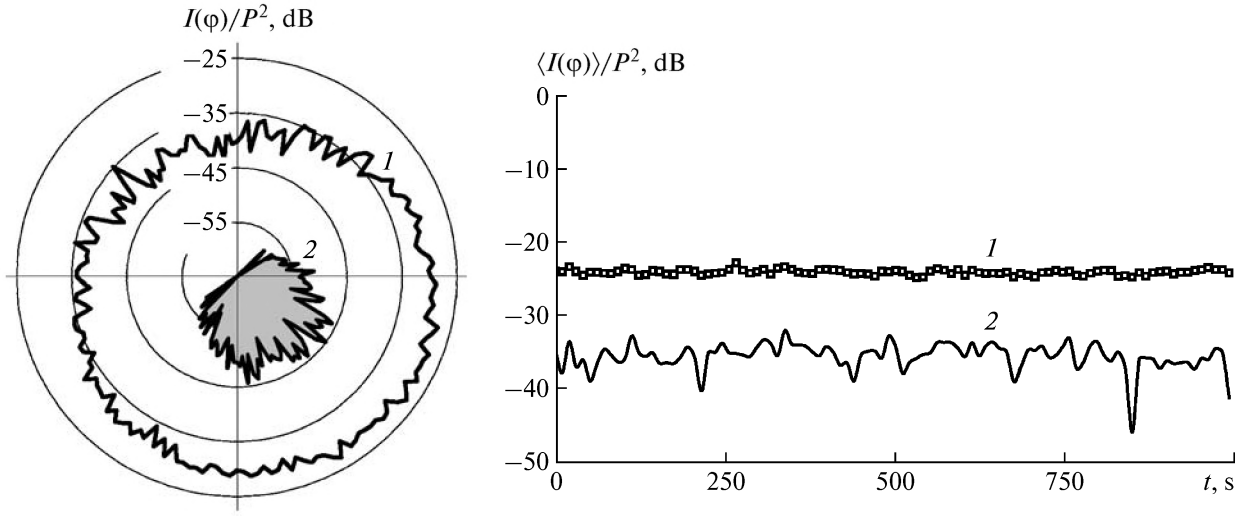

Fig. 4. Noise intensity distributions in the White sea area as functions of time: spatial distribution $I(\varphi)$ normalized to P^2 and distribution $\langle I(\varphi)\rangle$ averaged over the angle φ in the frequency range 78–315 Hz obtained using (*1*) algorithm I and (*2*) algorithm II.

For the values of $I(\varphi)$ in Fig. 4 the following condition is well satisfied: $\sum_{n=1}^{360} I(\varphi_n) = 1$, i.e., the integral intensity's level is equal to P^2.

The dependence $I(\varphi)$ constructed using algorithm II reflects the spatial distribution of the relatively stable in the horizontal plane anisotropic component of the acoustic power flux's vector for the noise field whose integral level for this area is γ_a = 13...15 dB, which is lower than P^2. This means that according to formal criteria, the single CRM possesses a fundamental capability of determining the direction toward rather weak localized sources with SNR in the pressure channel much lower than unity on the background of moderate isotropic noise fields. This property is based on the measuring of the characteristics of the acoustic field at one point.

However, some problems arise upon estimation of potential capabilities of separation of weak signals on the background of the noise of the water area. Thus, for example, for the above situation the acoustic power flux of the deterministic source with a signal level at the output of the single's omnidirectional hydrophone equal to the noise level of the water area should exceed the noise level in the angular sector of interest by γ_a = 13...15 dB. However, that is not so. Unlike the antenna array for which the value of γ_a indeed characterizes its noise immunity in the given angular sector, the value ΔI of excess of the signal from the localized source over the water area's noise (Fig. 3c) depends on a number of factors; the main of these factors is SNR for the acoustic power flux. Unlike the antenna array, the angular spectrum of energy arrival from the localized source determined using the above algorithms is rather broad, this is related with considerable space and time fluctuations of the total recorded vector $\mathbf{W}_S + \mathbf{W}_N$ formed with participation of the localized source. Obviously, as it was indicated above, the bearing angle's variance essentially depends on the ratio $|\mathbf{W}_S|/|\mathbf{W}_N|$. This certainly distinguishes the determination of the direction toward the source using CRM and the antenna array; therefore, usually additional processing of the envelope of the dependence $I(\varphi)$ is necessary for determination of the true bearing angle toward the source with the given precision, as well as for determination of the true radiation level of this source.

4. APPLICATION OF SONOGRAPHIC ANALYSIS METHODS WITH HIGH RESOLUTION FOR INCREASING NOISE IMMUNITY AND SPATIAL SEPARATION OF SEVERAL SOURCES IN THE WATER AREA

The bearing angle's variance can be decreased (therefore, the reliability of separation of the signal from the localized source on the background of ambient noise can be increased) due to the increased ratio $|\mathbf{W}_S|/|\mathbf{W}_N|$ (see Fig. 3), and the fluctuation component can be decreased due to the increased statistics. However, for moving objects the averaging time often cannot be considerably increased. Therefore, practically the only way of simultaneous satisfaction of both conditions is the increase in the number of analyzed frequency bands, i.e., higher frequency resolution of the spectral analysis. The same method in most practical cases allows one to spatially separate two and more real broad-band signal sources operating in the overlapping frequency bands. The latter is usually related with the possibility of separation of discrete noise components of most sea objects, which are always present.

However, as applied to the goal of this study, high frequency resolution imposes constraints on the possibility of separation of the weak signal on the background of ambient noise of the water area. In this case, two problems should be solved. The first one is related with the necessity of increasing the array of processed data for the narrow-band analysis. It is known that if standard Fast Fourier Transform algorithms are used, the width of the frequency band for analysis is inversely proportional to the sampling length. This means, for example, that while for operation in a frequency interval of 0–1000 Hz, a discretization frequency of 4000 Hz, and a frequency resolution of 1 Hz, a sampling with a length of 4000 samples per each channel is required, and for a frequency resolution of 0.05 Hz the sampling length should be 80000 samples. The second problem is the frequency fluctuations of the signal both due to the unstable operation of emitting mechanisms of the object and fluctuations of the signal propagation and due to the Doppler effect if the sought object moves.

The first problem is easily solved. For decreasing the amount of the analyzed sampling, the so called digital quadrature and low-frequency decimation filtering can be used which are usually designated for preliminary signal processing necessary for realization of algorithms of spectral and sonographic analysis with high frequency resolution.

Quadrature filtering (complex demodulation) of signals is the method used in signal processing problems, in which some segment of the signal spectrum within the frequency interval $\{f_c; f_c + f_n\}$ [22], is useful for the considered problem. This filtering is realized by multiplication of the initial signal $U(i\Delta t)$, discretely digitized with the quantization frequency $f_d = 1/\Delta t$ (Δt is the time interval of initial quantization) by the complex exponent $\exp(j2\pi f_c i\Delta t)$ and subsequent bounding of the low-frequency filtering of the signal from above by the frequency f_n, which is applied to the real and imaginary parts of the result of multiplication. Here, f_c is the lower bound of the analyzed frequency interval, $j = \sqrt{-1}$.

As a result of multiplication of the signal $U(i\Delta t)$ by the complex exponent, the neighborhood of its spectrum with the center determined by the exponent frequency f_c is transmitted to the zero frequency region. Then, the signal is filtered using the low frequency filter with the cutting frequency f_n (boundary of the stopping frequency of the low frequency filter), and as a result only the spectral segment of interest within the frequency interval $\{f_c; f_c + f_n\}$ is preserved. Thus, the formed complex signal is usually called the complex envelope. Then, according to the bandwidth of low frequency filtering (Nyquist condition) the new quantization frequency f_D of the complex envelope is chosen, $f_D \geq 2f_n$. The choice of f_D is realized by decimation of samples of quadrature signal components at the outputs of the low frequency filters.

The result of quadrature decimation filtering is the complex signal, in which spectral characteristics of the initial signal in the filtering range $\{f_c; f_c + f_n\}$ realized in the frequency band from 0 to f_n, are preserved.

Then, the high resolution analysis of the spectral sonographic based on methods of time–frequency signal transformations is realized; it is described in detail, for example, in [22–24].

Three algorithms of such transformations are considered most often: the time–frequency representation based on the short-term Fourier transform (F algorithm); the time–frequency Wigner representation (W algorithm); and the time–frequency representation using the compensating function of the signal frequency's variation of the linear frequency modulated (LFM) type (Q algorithm). Each of these signal representations possesses its positive and negative features. This prevents the unambiguous selection of one of them.

The main parameter of high frequency resolution algorithms is the effective length of the weighting function $h(t)$ determining the effective length of the sliding time window, which is applied in spectral analysis for decreasing side lobes [25]. The choice of the effective length depends both on the high frequency resolution algorithm and the analyzed signal.

The time–frequency representation based on Fast Fourier Transform usually represents the sequence of Fourier spectra calculated for sequential segments (possibly overlapping) of the signal $U(t)$ with the sliding time window $h(t)$ with the effective length ΔT_{eff}. This representation possesses rather good noise immunity. The noise level for this representation is known [26] to decrease inversely proportional to the effective window length ΔT_{eff}, while the intensity of the narrow-band peak corresponding to the signal preserves, and therefore, SNR increases.

However, possible frequency variation of discrete components on the time interval of the window length results in the spectrum distortion ("smearing"). In this case, the frequency components of the spectrum are found in several frequency bands, which results in worsening SNR at the output and makes further reduction of the band for frequency analysis inefficient. Figure 5 shows the results of the model experiment on determination of the histogram $I(\varphi)$ (an angular resolution of 1°) for the harmonic signal with a frequency of 230 Hz on the background of noise isotropic in the horizontal plane with SNR in the pressure channel close to unity for different frequency resolution of spectral analysis $\delta f = 1$ Hz. The plots in Fig. 5a correspond to the signal which does not fluctuate with the frequency: curve *1*—1Hz; curve *2*—0.1 Hz; curve *3*—0.06 Hz; and curve *4*—0.03 Hz.

Figure 5b shows the results of estimates of Δ characterizing the reduction of the value of $I_{max}(\varphi)$ in the direction toward the signal source for different frequency resolutions δf of the standard Fast Fourier Transform for different frequency fluctuations of the signal from the localized source with respect to $I_{max}(\varphi)$ of the nonfluctuating signal. It can be seen that for the frequency-unstable signal already for a frequency analysis band of 0.1 Hz up to 10 dB in SNR may be lost. If the parameter α with the meaning of the variation rate of the instantaneous frequency of the useful narrow-band signal ($\omega = \omega_0 + \alpha t$) is introduced, for the window length ΔT_{eff} larger than $(2\pi/\alpha)^{1/2}$ the signal intensity drops inversely proportional to the window length, i.e., SNR does not further increase. In this sense the window length $\Delta T_{eff} = (2\pi/\alpha)^{1/2}$ for F algorithm should be considered optimal.

For the Wigner distribution on finite time intervals with the sliding time window $h(t, \omega)$ the specific feature is that, unlike the Fourier transform, the trajectory of the frequency–time trace of the LFM signal on the time–frequency plane is reproduced correctly. Using this distribution with the sliding time window it is possible to separate (nonparametric approximation) trajectories of frequency traces of multicomponent signals in the time–frequency plane, which vary according to practically any law. With decreasing effective size of the time window the resolution of the analysis, obviously, decreases.

For tone sources moving in a medium it was proposed in [27] to calculate the spectrum of the nonstationary signal in the interval [0, T] observed at the receiver as a function of two variables $S(\omega, \alpha)$. Here, similar to the above said, α is the parameter with the meaning of the variation rate of instantaneous frequency. The algorithm of spectrum estimation (Q algorithm) consists in the search of sample functions with respect to the parameter α and the choice of the effective integration interval T for achieving the compromise between the resolution, bias errors due to deviation of the instantaneous frequency's variation law from the linear one, and the noise immunity. This algorithm possesses higher noise immunity, as compared to the algorithm based on Wigner transform. The main disadvantage of this algorithm is the necessity of a priori solution of the compromise between the length of the time interval of the sample function and the required resolution in the case of essentially "curvilinear" trajectories of frequency–time traces and the necessity of performing a rather large search among the parameters of the sample functions.

For the same length of the time window the frequency resolution of the considered algorithms for the steady-state case ($\alpha = 0$) are related as $\Delta\omega_Q = 2\Delta\omega_F = 4\Delta\omega_W$. For nonstationary signals this relation changes in a more complex way. The specific feature of W and Q algorithms is that there is no optimal window for nonstationary signals in these algorithms, since with

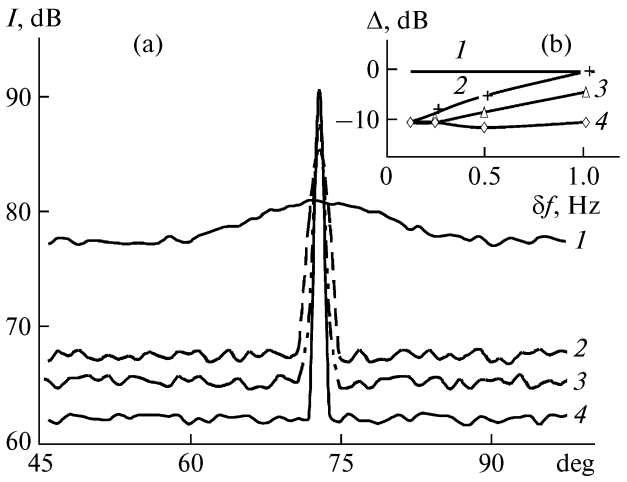

Fig. 5. Dependence $I(\varphi)$ for (a) harmonic signal nonfluctuating with respect to frequency for frequency resolution (*1*) 1, (*2*) 0.1, (*3*) 0.06, and (*4*) 0.03 Hz; (b) estimate of Δ of $I_{max}(\varphi)$ reduction with respect to recorded nonfluctuating harmonic signal for signal frequency fluctuation: (*1*) 0.01, (*2*) 0.5, (*3*) 1, and (*4*) 3 Hz.

the increasing window, both the frequency ($\Delta\omega \sim 1/T$) and time ($\Delta T \sim 1/(\alpha T)$) resolutions increase. In this case, the LFM signal's amplitude in the sonogram is preserved, and the noise level drops with increasing the window length. However, the degree of noise suppression in these algorithms is different.

For W sonograms the estimation of the noise level σ^2 can be expressed by the relation whose derivation is similar to that for the noise level in the correlation method of estimation of the narrow-band signal level [26], $\sigma_W^2 \sim \dfrac{A^2\sigma_\eta^2}{T} + \dfrac{\sigma_\eta^4}{T}$ (σ_η^2 is the noise level in the initial signal). For Q sonograms $\sigma_Q^2 \sim 1/\ln(T)$, i.e., in this case, the noise level in the sonogram drops much slower with increasing window length [24].

Obviously, in the case of the nonlinear dependence of frequency components of the signal on time the estimates of the amplitude of instantaneous frequencies become biased.

Figure 6 illustrates the sonograms of the real signal emitted in the neighborhood of 300 Hz by the source homogeneously moving past the receiving system calculated using the algorithm of short-term Fourier transform (Fig. 6a), based on the Wigner transform (Fig. 6b), and the algorithm with LFM compensation (Fig. 6c). In the case of the F algorithm, discrete component "traces" with a frequency of approximately 299 Hz are stronger smeared due to the Doppler frequency's variation on the signal's realization length.

The LFM-compensation-based algorithm possesses the best noise immunity. However, for its complete realization it was necessary to use a priori infor-

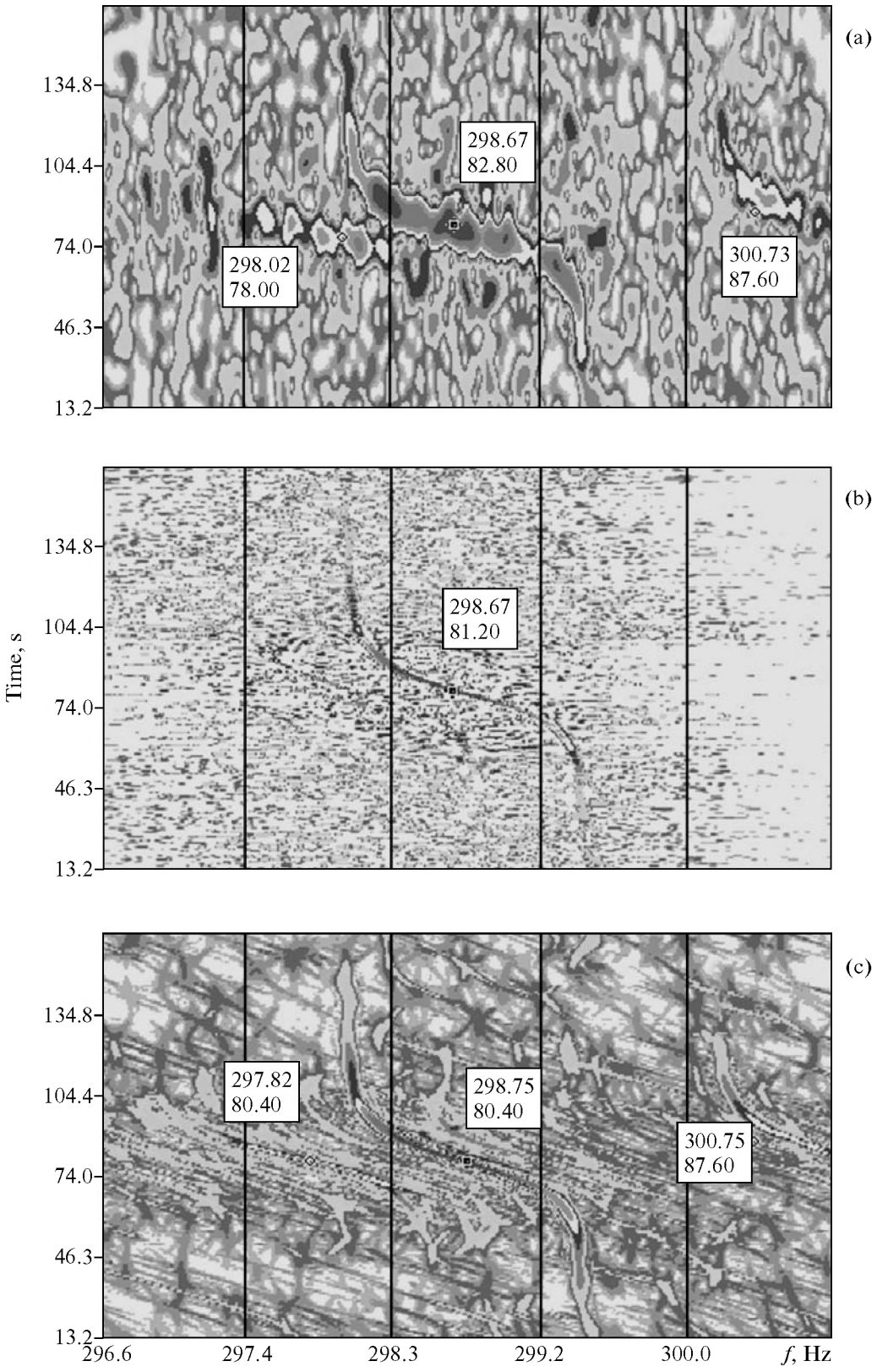

Fig. 6. Example of application of algorithms of sonographic analysis with high frequency resolution for real signal processing in the neighborhood of 300 Hz from a sea object uniformly moving past the receiving system: (a) F algorithm, analysis band $\delta f = 0.06$ Hz; (b) Wigner transform based algorithm, $\delta f = 0.03$ Hz; (c) algorithm using Fourier transform and LFM compensation, $\delta f = 0.06$ Hz. Numbers in rectangles show the traverse signal frequency and level.

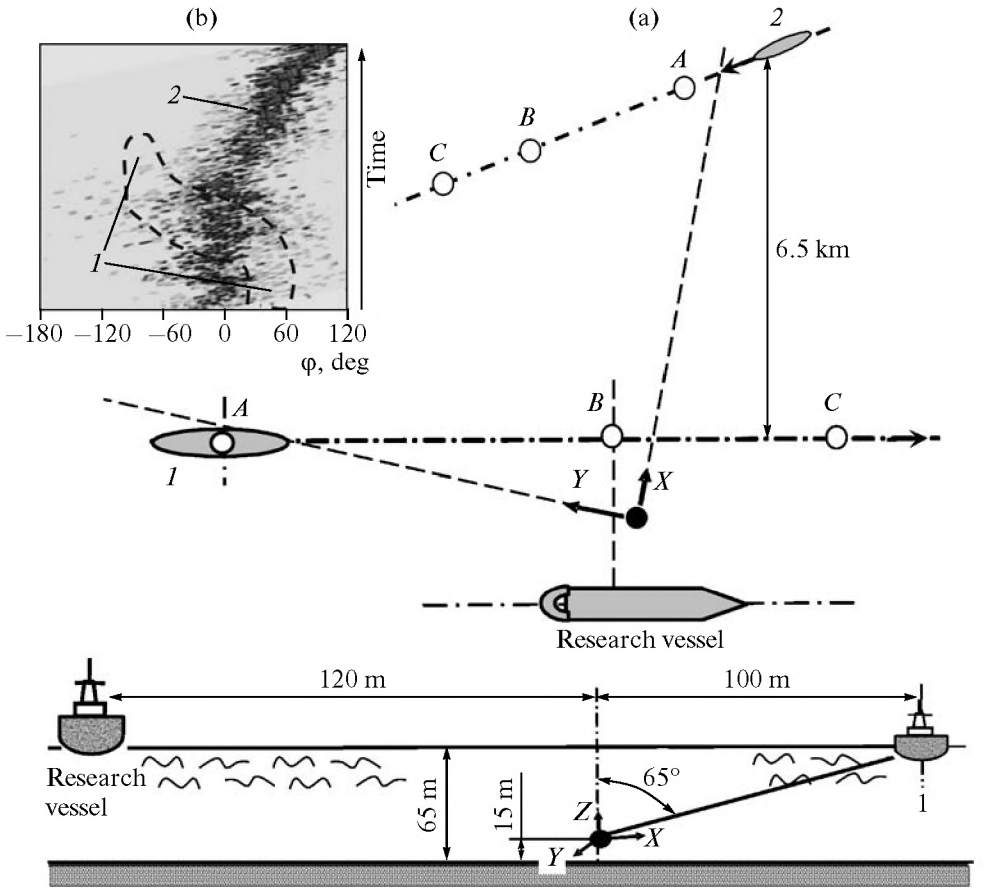

Fig. 7. (a) Schematic diagram of position of (*1*) low noise, (*2*) dry cargo, and receiving system installing (RSIS) ships in a shallow water area; and (b) example of sonogram in *azimuthal angle–time–intensity* coordinates in 1/3 octave 160 Hz calculated using algorithm I without frequency filtering of signals for frequency resolution $\delta f = 1$ Hz.

mation on the maximal variation rate and the assumed width of the discrete component.

Figure 7 shows the realization of quadrature filtering with subsequent high frequency resolution sonographic analysis for spatial separation according to algorithm I of two localized sources with overlapping radiation spectra in a shallow water area. A low-noise ship (characteristic traverse SNR in the pressure channel in the 1/3 octave 160 Hz band for a frequency resolution of 1 Hz of approximately 6–8 dB) served as one of the localized sources and the dry cargo ship (traverse SNR of 8–11 dB) as the other source. The schematic diagram of their mutual position at different times during the experiment is shown in Fig. 7a.

Figure 7b shows the "standard" sonogram in *azimuthal angle–time–intensity* coordinates in 1/3 octave 160 Hz calculated using algorithm I without frequency filtering of signals for the frequency resolution $\delta f =$ 1 Hz. Due to the considerable difference in the radiation levels only the transit characteristic of the most powerful signal source, the dry cargo ship, was clearly manifested in the sonogram.

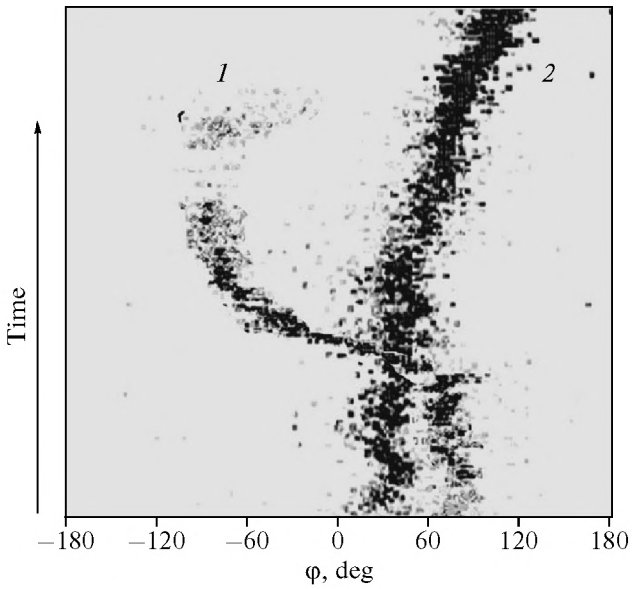

Fig. 8. Example of sonogram in 1.3 octave 160 Hz in *azimuthal angle–time–intensity* coordinates calculated using algorithm I with digital quadrature and low frequency decimation filtering for frequency resolution $\delta f = 0.1$ Hz: (*1*) low noise; (*2*) dry cargo ships.

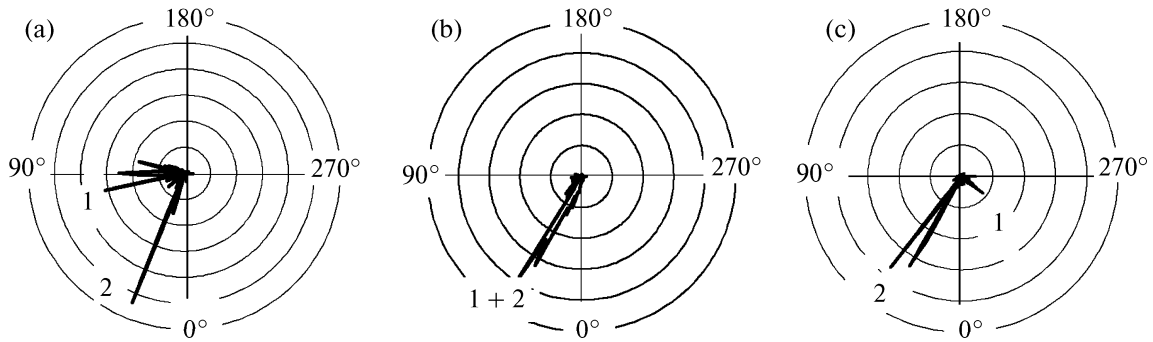

Fig. 9. Examples of spatial separation of signals for two moving local sources: (1) low-noise ship and (2) dry cargo ship in the horizontal plane in 1/3 octave 160 Hz for 10 s averaging using the digital quadrature and low frequency decimation filtering for three time instants shown in Fig. 7: (a) point *A*; (b) point *B*; and (c) point *C*.

For spectral analysis with relatively high frequency resolution (δf of tenth fractions of Hz) and algorithm I it turned out natural that discrete components of radiation of different objects (including secondary reflected object signals) were separated with respect to frequency, and as a consequence, the spatial spectra of the acoustic power flux's vector for different sources were also separated with respect to the angles of arrival. As a result, for statistical narrow-band analysis of the spatial distribution of the vector $\mathbf{W}_R$ each of the objects in the water area provided a separate transit characteristic (Fig. 8). Note that the spread of bearing angles is due to the same reasons discussed above. Selected results of determination of bearing angles toward sea objects situated at points *A*, *B*, and *C* of motion trajectories (see Fig. 7) are given in Fig. 9.

5. CONCLUSIONS

The presented experimental data demonstrate that the application of multicomponent combined receivers or CRMs considerably extends the capabilities of small-size receiving hydroacoustic systems in investigation of the signal–noise situation in the water area. At the same time, the following issues discussed in this paper should be mentioned separately.

(1) CRM cannot replace in full, measure extended antenna arrays based on hydrophones in the investigation of spatial noise spectra of the water area.

(2) Under certain conditions *upon solution of particular applied problems*, especially in the low frequency and subsonic ranges, for which it is difficult to create antenna arrays with "good" spatial resolution, the spatial distribution of the acoustic power flux's vector can be used for estimation (with some constraints) of the spatial noise spectrum of the water area.

(3) In spite of the relatively "obtuse" directional response pattern of separate channels of the vector receiver, the combined receiving module provides rather precise determination of the bearing angle for the localized source on the background of the water area's noise, including for SNR at the input in the pressure channel much lower than unity.

(4) The application of methods of sonographic analysis with high frequency resolution provides higher SRM noise immunity and distinguishes several localized sea objects simultaneously present in the water area.

REFERENCES

1. V. A. Gordienko, *Vector Phase Methods in Acoustics* (Fizmatlit, Moscow, 2007) [in Russian].
2. J. Clark and G. Tarasek, in *Proc. of the Oceans'06, MTS IEEE, Revolutionize Marine Sci. Technology, Sept. 18–21, 2006* (Hynes Convention Center, Boston, Massachusetts, 2006).
3. J. L. Pascal, Rev. Pract. Contr. Dustriel **21**, 3840 (1982).
4. J.-A. Roy, in *Proc. of the UDT Pacific 98, Feb. 1998* (Sydney, Australia, 1998), pp. 290–295.
5. V. K. Maslov and A. M. Trokhan, *Trudy VNIIFTRI*, vyp. 47 (139) (VNIIFTRI, Moscow, 2004), pp. 84–131.
6. V. K. Maslov, *Trudy VNIIFTRI*, vyp. 47 (139) (VNIIFTRI, Moscow, 2006), pp. 77–133.
7. V. I. Korenbaum, Akust. Zh. **41**, 930 (1995) [Acoust. Phys. **41**, 825 (1995)].
8. S. D. Vorob'ev and V. I. Sizov, Akust. Zh. **38**, 654 (1992) [Sov. Phys. Acoust. **38**, 361 (1992)].
9. M. D. Smaryshev, Akust. Zh. **51**, 357 (2005) [Acoust. Phys. **51**, 477 (2005)].
10. V. I. Klyachkin, Akust. Zh. **50**, 516 (2004) [Acoust. Phys. **50**, 438 (2004)].
11. V. A. Gordienko and B. I. Goncharenko, Vestn. Mosc. Gos. Univ., Ser. Fiz. Astron. **35** (6), 93 (1994).
12. V. A. Gordienko and V. I. Il'ichev, Dokl. Akad. Nauk **339**, 675 (1994).
13. V. A. Gordienko and V. I. Il'ichev, Dokl. Akad. Nauk **340,** 408 (1995) [Dokl. Phys. **40**, 47 (1994)].
14. *Hydroacoustical Measurements. Terms and Definitions. Recomendations in Metrology* R50.2.037-2004 (Gosstandart Rossii, Moscow, 2004), p. 6.

15. A. N. Zhukov, A. N. Ivannikov, and V. N. Pavlov, Akust. Zh. **36**, 447 (1990) [Sov. Phys. Acoust. **36**, 249 (1990)].

16. V. A. Burov and E. E. Kasatkina, Akust. Zh. **43**, 22 (1997) [Acoust. Phys. **43**, 24 (1997)].

17. M. V. Andersen and R. L. Tittle, J. Acoust. Soc. Am. **45**, 1129 (1969).

18. V. A. Gordienko, Ya. A. Ilyushin, and V. I. Il'ichev, Dokl. Akad. Nauk **339**, 808 (1994).

19. V. A. Gordienko, V. N. Nekrasov, B. I. Goncharenko, et al., in *Problems and Methods of Hydroacoustic Measurements, Collected Vol. of FGUP VNIIFTRI* (VNIIFTRI, Moscow, 2003), pp. 161–210.

20. *Sound Intensity Analyzer Type 2134, Instruction Manual* (Bruel & Kjer, 1983).

21. V. A. Gordienko, E. L. Gordienko, N. V. Krasnopistsev, and V. N. Nekrasov, Akust. Zh. **54**, 774 (2008) [Acoust. Phys. **54**, 670 (2008)].

22. L. Cohen, TIIER **77** (10), 72 (1989).

23. V. K. Maslov, in *Tomographic Methods in Physico-Technical Measurements, Collected vol. of NPO VNIIFTRI* (VNIIFTRI, Moscow, 1990), pp. 56–85.

24. V. N. Toropov, in *Tomographic Methods in Physico-Technical Measurements, Collected vol. of NPO VNIIFTRI* (VNIIFTRI, Moscow, 1990), pp. 97–102.

25. F. J. Harris, TIIER **66** (1), 60 (1978).

26. J. Max, *Methods and Techniques for Processing Signals in Physical Measurements* (Mir, Moscow, 1983), vol. 1 [in Russian].

27. M. A. Price, *Progress in Underwater Acoustics* (Plenum, New York, 1987), p. 735.